.

Error quantification in calibration of AFM probes due to non-uniform cantilevers

Hendrik Frentrup[1], Matthew S. Allen[2]

[1] Graduate Student, Universität Stuttgart, Germany
Institute of Applied and Experimental Mechanics (IAM), Pfaffenwaldring 9, 70550 Stuttgart
hendrik.frentrup@gmail.com

[2] Assistant Professor, University of Wisconsin-Madison
535 ERB, 1500 Engineering Drive, Madison, WI 53706
msallen@engr.wisc.edu

Abstract

For more than two decades, the Atomic Force Microscope (AFM) has provided valuable insights in nanoscale phenomena, and it is now widely employed by scientists from various disciplines. AFMs use a cantilever beam with a sharp tip to scan the surface of a sample both to image it and to perform mechanical testing. The AFM measures the deflection of the probe beam so one must first find the spring constant of the cantilever in order to estimate the force between the sample and the probe tip. Commonly applied calibration methods regard the probe as a uniform cantilever, neglecting the tip mass and any non-uniformity in the thickness along the length of the beam. This work explores these issues, recognizing that dynamic calibration boils down to finding the modal parameters of a dynamic model for a cantilever from experimental measurements and then using those parameters to estimate the static stiffness of a probe; if the modes of the cantilever are not what was expected, for example because the non-uniformity was neglected, then the calibration will be in error. This work explores the influence of variation in the thickness of a cantilever probe along its length on its static stiffness as well as its dynamics, seeking to determine when the uniform beam model that is traditionally employed is not valid and how one can ascertain whether the model is valid from measurable quantities. The results show that the Sader method is quite robust to non-uniformity so long as only the first dynamic mode is used in the calibration. The thermal method gives significant errors for the non-uniform probe studied here.

Nomenclature			
α_n	n^{th} frequency parameter	M	Moment
b	cantilever width	ψ_n	n^{th} mode shape
E	Young's modulus	ω_n	natural frequency
F	force	Q	quality factor
Γ	hydrodynamic function	ρ	cantilever density
h	cantilever thickness	ρ_{f}	density of the surrounding fluid
I	second moment of area	T	temperature
k_{s}	spring constant	w	deflection
k_{B}	Boltzmann's constant	W	static deflection
L	cantilever length	χ	optical lever factor
m	mass	x	coordinate along beam axis

1 Introduction

Originally designed to measure conductors and insulators on an atomic scale, the inventors of the Atomic Force Microscope (AFM) envisioned a device that can be applied to measure forces and examine surfaces in many fields of science [1]. One great advantage of the AFM is the fact that the sample of interest need not be coated, measured in vacuum or conduct an electrical current. AFMs can operate under ambient conditions. Hence, the range of applications for an AFM are enormous and allow quantitative research on the nanoscale where other microscopic methods are far beyond their limits. Today, the AFM is indeed useful to scientists in the fields of medicine, biotechnology, chemistry, engineering and many more.

A particularly spectacular example for the potential of AFM is the imaging of single atoms within a pentacen molecule [2]. It is necessary to perform the imaging at nearly absolute zero and sharpen the tip of the AFM by picking up a CO molecule to achieve this resolution level. Nonetheless, these dimensions were only explored in a theoretical realm before. Recently, the AFM also rendered possible the manipulation of single atoms on a semiconductor surface at room temperature [3]. Sugimoto et al. [3] describe how they implemented co-called dip-pen nanolithography with the AFM. The tip apex is wetted with atoms which could then be individually deposited to write patterns on the semiconductor surface. These examples show how important of a role the AFM plays in the development of nanoscale electronics and chemistry. Moreover, AFM techniques are commonly employed in microbiology for their advantage over electron microscopy when measuring living organisms. Only under conditions where the organisms prosper is it possible to directly observe their cell growth [4]. Hence, measurements on living cells have to be done in aqueous solutions in order to observe dynamic events on this scale, such as the interaction between cell membranes and drugs [5]. Structural imaging being one usage, force spectroscopy is also increasingly being used in microbiology to measure the nanoscale chemical and physical properties of cells. The practical potential of force spectroscopy is demonstrated in a study on the nanomechanical properties of cancer cells [6]. AFM indentation on metastatic cancer cells discovered a significantly lower stiffness compared to benign cells despite their morphological similarity, suggesting that the AFM might be more effective for cancer screening than visual inspection of the cells.

The AFM uses a sharp tip mounted on a small cantilever beam to scan over the surface of a sample. While scanning the sample, the deflection of the microcantilever is measured by pointing a laser at its free end and recording the motion of the reflected laser spot with a photodiode [5]. With help from a calibration sample, it is possible to determine the relationship between the voltage output of the diode and the cantilever's deflection, called deflection sensitivity.

A second calibration must be performed if one wishes to relate the measured deflection to the tip-sample force. This second calibration is the focus of this work. Since the deflections of the cantilever are linear, the spring constant, i.e. the static stiffness of the cantilever, is the parameter that must be determined to find the forces of interest. In classical beam theory, the spring constant[1] of a uniform cantilever $k_{\mathrm{s}} = Ebh^3/4L^3$ depends on its Young's modulus E and it's geometry, with b being the cantilever's width, L its length [7]. The thickness of the beam, h, is typically assumed to be uniform along the length. Due to considerable variations in microfabrication, the properties of the cantilevers, especially Young's modulus, thickness and mass distribution, cannot be determined very easily. Calibration is therefore of crucial importance in force spectroscopy, and even in routine contact-mode or friction force imaging if one needs to know the force applied by the probe during imaging.

1.1 Calibration methods

To be practical, AFM calibration methods must not damage the probes in the calibration process and one must be able to perform them quickly and without the need for additional complex equipment other than the AFM. Moreover, effective calibration methods must be applicable under ambient conditions as

---

[1] In detail, $k_{\mathrm{s}} = 3EI/L^3$, where I is the beam's second moment of area $I = bh^3/12$.

the AFM usually operates at such. The focus of this work is on two non-destructive, dynamic calibration methods, the Sader method and the Thermal Tune method. Sader developed his method by taking the effects of a surrounding fluid on the oscillating cantilever into account [8]. He uses the natural frequency and Q factor of the first mode of the cantilever to determine its static stiffness. Some information on the cantilever's geometry is required to use the Sader method, namely the planview dimensions of a rectangular cantilever, i.e. the width and length, which govern the effects of the fluid for flexural oscillations. The planview dimensions can be easily determined using optical microscopy and therefore this does not pose a severe limitation for the calibration. However, Sader assumed a uniformly thick cantilever in his derivation and did not take a tip mass into account. Allen et al. [9] pointed out that these assumptions are not accurate and, depending on the mode used for the calibration, can lead to errors of considerable extent in the calibration process. They quantified the error in the stiffness estimated by the Sader method due to an unmodeled rigid tip and proposed a method that can be used to estimate the tip mass from measurements of the natural frequencies of the probe. The tip was found to cause considerable calibration error for some AFM probes if not correctly accounted for. This work uses a similar approach to explore the effect of a non-uniform thickness along the beam's length on the dynamic properties of the cantilever, which influence the accuracy of the calibration.

The Thermal Tune method, first proposed by Hutter and Bechhoefer [10] exploited the equipartition theorem to determine the spring constant. The theorem states that the mean kinetic or potential energy of each mode of a cantilever when excited by only thermal noise is equal to $1/2\ k_{\mathrm{B}}T$ [11], with T being the temperature and k_{B} being Boltzmann's constant. This relationship is used to relate the mean thermal oscillation amplitude with the spring constant. The method is quite simple, although there are a number of important details that must be accounted for, as described by Cook et al. [12].

2 Effects of Non-uniform Thickness on Dynamic Properties

Many commercially available AFM probes are significantly non-uniform along their lengths. For example, the SEM images shown below were obtained from a CSC38-B cantilever manufactured by Mikromasch. The nominal thickness of the beam is given by the manufacturer as $1\ \mu$m. Scanning Electron Microscope (SEM) images indicate that the thickness of the cantilever is not uniform but has a considerable taper toward the tip. It is almost three times as thick as nominal at the point where the tip starts. The profile of the beam was estimated using these SEM images and will be used to quantify the effect of this thickness non-uniformity on calibration for this particular probe, with a view to extending the methodology to other probes.

(a)   (b)
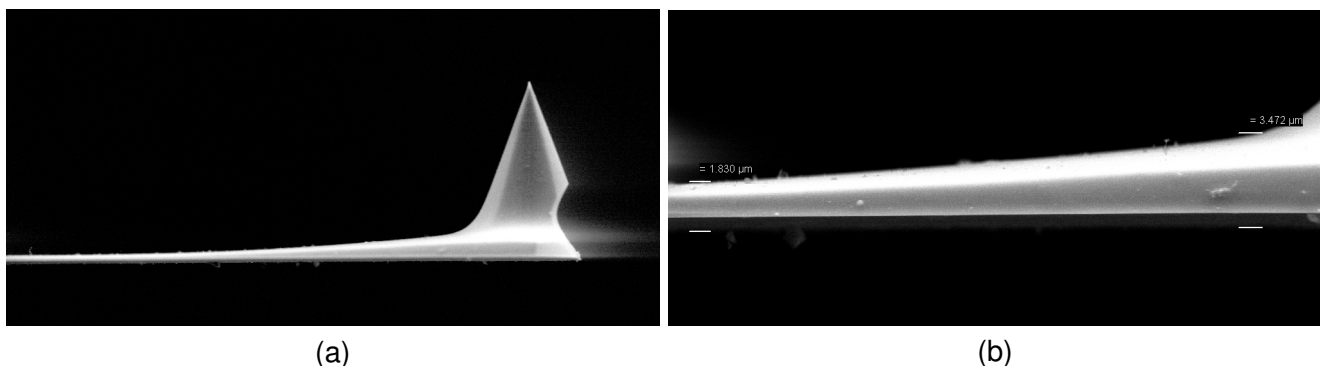
Figure 1: SEM images of a silicon nitride cantilever beam. On the left, the tip and a portion of the cantilever are shown. In (b), a detail near the tip is shown where it can be observed how the thickness of the cantilever increases from 1.830 μm to 3.472 μm toward the tip.
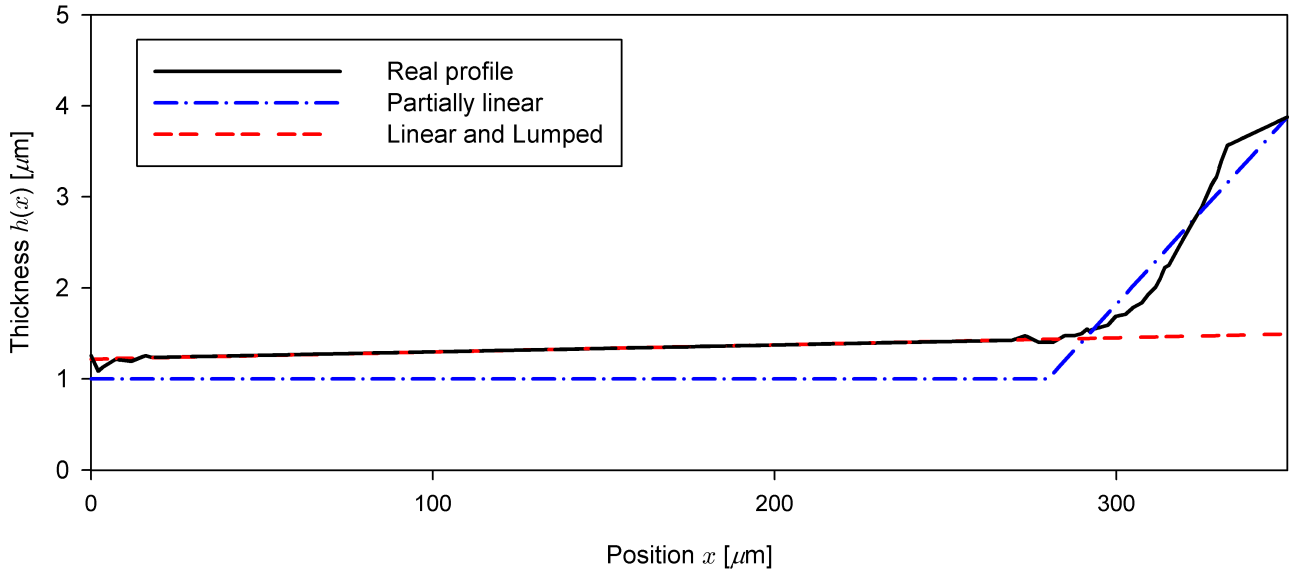
Figure 2: Different thickness profiles of the cantilever beam. The estimate of the actual profile and two fitted counterparts are shown

The mechanics of the measured cantilever profile will also be compared to two different profiles that approximate it with a small number of parameters. The first models the non-uniformity with a section that has constant thickness, h_{nom} with a taper starting at x_0, and reaches the same thickness as the real cantilever at the free end. This profile will be called the "partially linear" profile. The second models the non-uniformity as a linearly increasing thickness. This profile cannot mimic the prominent increase in thickness that the real profile has at the end of the cantilever, so that part is regarded as an extra mass without rotary inertia and lumped at the end of the cantilever. This latter profile shall be referred to as "linear and lumped". Both profiles are defined by only three parameters, which are given in Table 1. The "linear and lumped #2" profile is a result of the sensitivity analysis shown in Figure 4. Its parameters were chosen to match the experimental result of the frequency spacing more closely, whereas the parameters for the "linear and lumped" profile were chosen based on the SEM images shown previously. More complicated profile models could be envisioned, but then one would have more free parameters that must be either assumed or determined.

Profile parameters			
Partially linear	$h_{\mathrm{nom}} = 1.0\,\mu$m	$h(1) = 3.876\,\mu$m	$x_0 = 0.83$
Linear and lumped	$h_0 = 1.218\,\mu$m	$h_1 = 0.275\,\mu$m	$\Delta m = 5.792 \cdot 10^{-12}$ kg
Linear and lumped #2	$h_0 = 1.193\,\mu$m	$h_1 = 0.302\,\mu$m	$\Delta m = 6.372 \cdot 10^{-12}$ kg

Table 1: The parameters of the two chosen profiles fitted to the real cantilever profile. The definition of the parameters is given in section 6.1
of the appendix.

A Ritz model will be created for each of these probes, so the equations of motion governing the motion of the cantilever are given as follows, where $\mathbf{q}$ denotes the frequency domain amplitude of the generalized

coordinates [13]. The inertia and stiffness of the beam as well as the virtual mass added by the fluid and the dissipative effect of the fluid are included in the calculations (see section 6.2 in the appendix for details).

$$-\omega^2[\mathbf{M}]\mathbf{q} + \mathrm{i}\omega[\mathbf{C}]\mathbf{q} + [\mathbf{K}]\mathbf{q} = 0 \tag{1}$$

The Ritz method can be used to obtain approximate solutions for the mode shapes and natural frequencies of continuous structures. Here this approach is used to find the approximate mode shapes of non-uniform cantilevers. However, later we shall make use of the fact that a single term Ritz model is an exact model for the contribution of a single mode to a structure's response if the mode shape used in the Ritz series is exact.

The analytical model presented in [9] gives the mode shapes of a uniform cantilever [13] with a rigid tip on its free end. Those analytical mode shapes will be used in this work as basis functions for the Ritz method in order to find the modes of the cantilever for each of the thickness profile models in Table 1.

$$\phi_n(x) = \sin(\alpha_n x) + \sinh(\alpha_n x) + R_n\left(\cos(\alpha_n x) - \cosh(\alpha_n x)\right) \tag{2}$$

$$R_n = \frac{\sin(\alpha_n) + \sinh(\alpha_n)}{\cos(\alpha_n) - \cosh(\alpha_n)}$$

The parameters α_n depend on the boundary conditions which include the effect of the tip. In order to account for non-uniformity, the model used here allows for a variable thickness along the cantilever's length, $h = h(x)$.
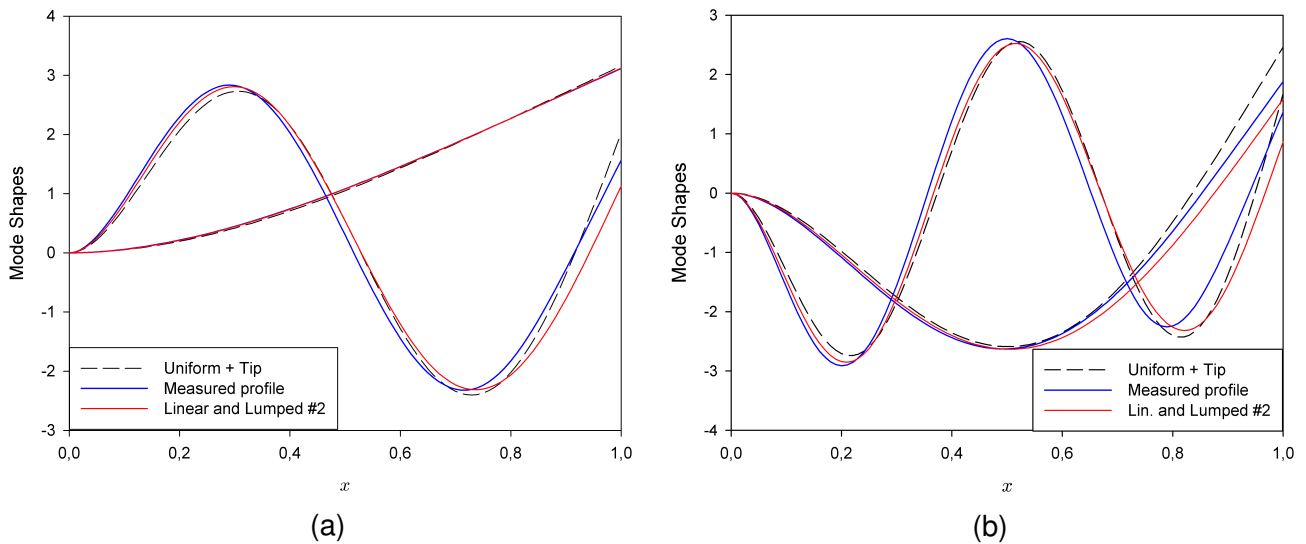

Figure 3: Mode shapes of the cantilever. The dashed lines depict the analytical mode shapes of a uniform cantilever with tip - solid lines are Ritz estimates of the mode shapes for the measured profile and for the "linear and lumped #2" profile. The odd modes are shown in (a), even modes in (b).

Figure 3 shows the mode shapes of a cantilever with a tip mass of $m_{\mathrm{r}} = 0.088$ and a uniform nominal thickness compared to those with the same tip and the thickness profile estimated from the SEM images. The third set of mode shapes shown are for the "linear and lumped #2" model described previously. The mode shapes in Figure 3 indicate lower amplitudes of vibration at the end of the beam for the "linear and lumped #2" cantilever profile than for the other two because the additionally lumped mass increases the

inertia of the beam at the free end. Also, the higher the order of the mode, the more the respective mode shapes are curved, in particular close to the free end of the beam, so thickness non-uniformity has a more prominent effect on the higher modes.

	ω_2/ω_1	δ_{exp}	ω_3/ω_1	δ_{exp}	ω_4/ω_1	δ_{exp}
Experimental [9]	7.806	-	23.572	-	48.490	-
Uniform + Tip	6.475	17.05%	18.507	21.49%	36.826	24.05%
Measured profile	7.807	0.01%	23.665	0.39%	48.409	0.17%
Partially linear	7.813	0.09%	23.698	0.53%	48.964	0.98%
Linear and lumped	7.658	1.89%	23.056	2.19%	46.771	3.54%
Linear and lumped #2	7.812	0.08%	23.642	0.30%	48.042	0.92%

Table 2: Frequency spacings of the cantilever beam. δ_{exp} is the deviation of the respective frequency spacing compared to the experimental value.

The spacings between the natural frequencies for all of these models are shown in Table 2. By comparing the frequency spacings rather than the frequencies, the comparison is not dependent on the modulus, density, and other physical properties of the probe. The analytical model underestimates the spacings between the modes considerably and with increasing deviation for higher modes. The model that uses the measured profile reproduces the frequency spacings with a very high accuracy. The partially linear profile is almost as accurate as the measured profile while the "linear and lumped" profile presents higher deviations, but both are significantly more accurate than the uniform model with a tip. The parameters for the "linear and lumped #2" model were chosen to minimize the difference in the frequency spacings, so the agreement is excellent. One can achieve good agreement in terms of the frequency spacings for both ways of parameterization. However, as shown below, the partially linear profile was found to erroneously represent the static properties of the measured profile, so the "linear and lumped" profile is of primary interest. Figure 4 depicts the sensitivity of the "linear and lumped" profile. The point of origin for the analysis was the initial set of parameters for this profile given in Table 1 and all three parameters were varied between 90 to 120% of their initial value. The starting thickness h_0 of the profile has proportionally higher influence on the frequency spacings than the other two parameters and is therefore varied to a lesser extent. The graph shows that it is not possible to match the frequency spacing of the measured profile in all four modes exactly, but it is very well possible to lower the deviation considerably. The second set of parameters for the "linear and lumped" profile given in Table 1 were found by using this sensitivity information to achieve better agreement.

In order to determine how well each of these models captures the static stiffness of the cantilever, an analytical solution was derived for the spring constant of a cantilever with an arbitrary thickness variation along its length. The deflection curve of the cantilever is given by $w'' = M(x)/EI(x)$. Loaded with a static tip force, the bending moment is linear. Thus, we can express the spring constant as follows

$$k_{\mathrm{s}} = \frac{Ebh_{\mathrm{es}}^3}{4L^3}, \tag{3}$$

$$h_{\mathrm{es}}^3 = -\frac{1}{3} \left[\int_0^1 \int_0^x \frac{(x-1)}{h(x)^3} \mathrm{d}x\mathrm{d}x \right]^{-1}. \tag{4}$$

The static stiffnesses computed for each of the probe models using this approach are shown in Table 3. The manufacturer estimated the spring constant of the cantilever at 0.03 N/m, presumably based on the
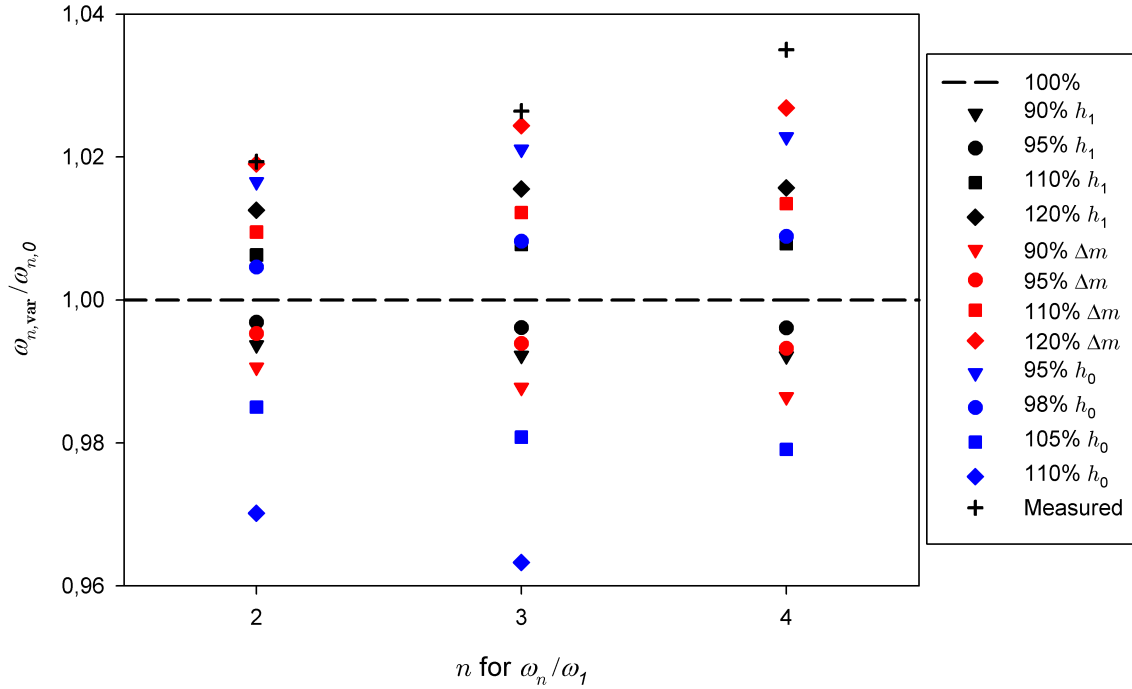
Figure 4: Variations in h_0, h_1 and Δm parameters of the "Linear and Lumped" profile showing the sensitivity of the frequency spacing with respect to these parameters.

Manufacturer's specification: $k_{\mathrm{s}} = 0.03\ (0.01 - 0.08)\ \mathrm{N/m}$	
	$k_{\mathrm{s}}\ [\mathrm{N/m}]$
Uniform + Tip	0.0278
Measured profile	0.0580
Partially linear	0.0278
Linear and lumped	0.0585
Linear and lumped #2	0.0560

Table 3: Static stiffness, k_{s}, estimated for each of the models of the thickness profile.

nominal thickness of $1\,\mu$m, and the analytical model agrees well with this. However, the manufacturer also states that the spring constant could be anywhere in the range from only a third to more than twice the nominal value. In fact, the profile from the SEM images has a spring constant of $0.058\,\mathrm{N/m}$ which is almost twice the nominal value. The other parameterizations of the model have a completely different static behavior. The considerable taper toward the free end of the beam has no noticeable effect on the beam's static stiffness as the "partially linear" spring constant is equal to that of the uniform cantilever. On the other hand, the static stiffness of the "linear and lumped" profile agrees very well with that of the measured profile.

3 Corrections of Calibration Methods

3.1 Sader Method

Modeling the cantilever with single mode, its first natural frequency, ω_1, depends on the mass m and the stiffness of the oscillator, $\omega_1^2 = k_s/m \Rightarrow k_s = M_e \rho h b L \omega_1^2$ [8]. With h, b, and L being the cantilevers thickness, width and length. The geometry of the cantilever and its density ρ are used to determine the mass. The expression presented by Sader treats the mass distribution as uniform along the length of the cantilever, so the effective normalized mass, M_e is equal to 0.2427 when $L/b > 5$ [14]. When vibrating in vacuum, this assumption is very accurate. However, an oscillating cantilever immersed in a fluid moves the surrounding fluid as it vibrates, creating an inertial loading on the beam, a virtual mass. The resonance frequencies of an immersed cantilever are lower compared to a cantilever in vacuum due to the inertial loading. The surrounding fluid also has a damping effect on the cantilever, which lowers the cantilever's quality factor Q, reduces the peak amplitude and broadens its resonance curve [15]. Sader accounted for the effects of the fluid by including a hydrodynamic force as part of the loading on the cantilever [16], based on the hydrodynamic function, Γ. By modeling the effect of the fluid, Sader was able to determine the mass and spring constant of the cantilever from the Q-factor and resonance frequency according to $k_s = 0.1906 \rho_f b^2 L \Gamma_i Q \omega_1^2$ [14], where ρ_f denotes the density of the surrounding fluid.

Following the approach in [9], the Sader method can be modified to include the effect of a massive tip and a non-uniform thickness. To this end, we introduce an equivalent thickness with respect to stiffness and inertia, h_{ek}^3 and h_{em} which are the following,

$$h_{ek,n}^3 = \frac{\int_0^1 h(x)^3 \left(\psi_n''\right)^2 \mathrm{d}x}{\int_0^1 \left(\psi_n''\right)^2 \mathrm{d}x} \qquad\qquad h_{em} = \frac{\int_0^1 h(x) \left(\psi_n\right)^2 \mathrm{d}x}{\int_0^1 \left(\psi_n\right)^2 \mathrm{d}x} \tag{5}$$

so that we can keep the original coefficients m_{nn} and k_{nn}. The prime in equation (5), denotes differentiation with respect to x. The equivalent thicknesses, h_{em} and h_{ek}, are the thicknesses that a uniform cantilever must have to produce the same m_{nn} and k_{nn} terms in a single-term Ritz model. Therefore, we can replace h^3 with h_{ek}^3 and h with h_{em} in the stiffness and inertial coefficients in section 6.2 of the appendix, and after some algebra one obtains the following equation for the static stiffness of the probe.

$$k_{s,Sader} = \frac{3\pi}{4} \rho_f b^2 L \Gamma_i \left(\frac{h_{es}}{h_{ek,n}}\right)^3 \frac{m_{nn}}{k_{nn}} Q \omega_n^2 \tag{6}$$

This expression is also valid for a uniform probe with a rigid tip, as presented in [9], and for a uniform probe without a tip it reduces to the formula given by Sader. If the thickness profile of a probe is known, then one can compute h_{es}, and with the mode shapes one can compute m_{nn}, k_{nn}, and $h_{ek,n}$. Then, this expression would give an accurate estimate of the spring constant, even in the presence of non-uniformity. Unfortunately, these quantities are not known in practice, so it is difficult to determine the needed constants. One must, instead, make a simplifying assumption regarding the cantilever, such as uniform thickness, in order to obtain an estimate for k_s. Our primary purpose for deriving eq. (6) is to estimate the error incurred by such an assumption. Consider an exact solution for the thickness profile and mode shapes. Denote the parameters for that model as h_{es}, $h_{ek,n}$, m_{nn}, and k_{nn}. These parameters would produce the true static stiffness if used in conjunction with the measured Q and ω_n. An approximate model gives different values for these parameters, which shall be distinguished with hats (ˆ). Then, the error incurred in the Sader method due to the simplifying assumption is given by the following.

$$\delta k_{s,Sader} = \frac{\hat{k}_{s,model} - k_{s,true}}{k_{s,true}} = \left(\frac{\hat{h}_{es} \, h_{ek,n}}{h_{es} \, \hat{h}_{ek,n}}\right)^3 \frac{\hat{m}_{nn}}{m_{nn}} \frac{k_{nn}}{\hat{k}_{nn}} - 1 \tag{7}$$

The Ritz mode shapes found previously for the measured profile were found to correspond well with the experimentally measured mode shapes shown in [17], so that model will be assumed to be exact

δk_{s}	Mode 1	Mode 2	Mode 3	Mode 4
Uniform No Tip - Measured	-2.22%	2.62%	6.24%	14.23%
Uniform + Tip - Measured	-2.71%	4.14%	15.91%	25.38%
Linear and Lumped - Measured	-0.06%	5.91%	10.52%	15.43%
Linear and Lumped #2 - Measured	-0.22%	6.00%	9.66%	14.09%

Table 4: Error in the static stiffness estimated by the method of Sader for various profiles as a function of the mode number used in the calibration. The model based on the measured profile was taken to be exact.

and used to compute the error in approximating the probe with each of the models listed in Table 1. The resulting relative errors for each of the models are given in Table 4. One observes that each of the models is capable of estimating the static stiffness of the probe to within 3% if the first mode is used in the calibration, and to within 6% if the second is used, although the errors become significantly larger if modes 3 or 4 are used. These modes are more sensitive because the tip mass and the stiffened section of the probe near the tip begins to have an important effect on the mode shapes. It is also interesting to note that the original original Sader model of a uniform beam without tip has smaller deviations from the measured profile than the model with a tip. Considering that the tip adds inertia to the model, Sader's original uniform cantilever is less stiff and lacks the inertial effect of the tip at the same time, leading to a mutual compensation in the calibration process and less deviation.

3.2 Thermal Tune Method

The Thermal Tune method is based on equivalence between the mean-square potential energy of the cantilever and $^1\!/_2\, k_{\mathrm{B}}\, T$.

$$\langle E_{\mathrm{vib}}\rangle = \frac{1}{2}k_{\mathrm{B}}\, T = \frac{1}{2}\left\langle \int_0^L EI(x)\left(\frac{\partial^2 w}{\partial x^2}\right)^2 \mathrm{d}x \right\rangle \tag{8}$$

The kinetic energy is related to the motion of the tip of the cantilever, which is related to the output signal of the photodiode. However, the sensitivity of the photodiode is measured under static conditions and the shape of a cantilever under static loading is different from its shape when vibrating freely. This is accounted for using the method described by Cook et al. [12], which multiplies the deflection measured by the photodetector, d_{c}^*, with the factor χ to yield the actual deflection needed for the calibration, d_{c}. The slope of the cantilever at x_1, where the laser is reflected on the beam, determines the laser spot's position on the photodetector [12]. Hence, χ depends on the ratio of the end-loaded slope W'_{end} to the freely oscillating slope W'_{free}

$$\chi(x_1) = \frac{W'_{\mathrm{end}}(x_1)}{W'_{\mathrm{free}}(x_1)}. \tag{9}$$

W is the cantilever's normalized shape[2], i.e. the normalized deflection curve in case of the end-loaded cantilever [12] and the normalized mode shape of a freely vibrating cantilever is given by $W_{\mathrm{free}}(x) = \psi(x)/\psi(1)$. Following the same approach used to derive the modified Sader method, the Thermal Tune relationship between the static stiffness and the probe parameters is [17]

---

[2]Normalized shape implies $W(1) \equiv 1$.

$$k_{s,\text{Thermal}} = \frac{3k_\text{B}T}{\langle (d_\text{c}^*)^2 \rangle} \left(\frac{h_\text{es}}{h_\text{ek,n}} \right)^3 \left(\frac{\psi_n'(1)^2}{k_{nn} \left(W_\text{end}'(1) \right)^2} \right) \tag{10}$$

Likewise, the error induced by non-uniformity in the Thermal Tune method is

$$\delta k_{s,\text{Thermal}} = \frac{\hat{k}_{s,\text{model}} - k_{s,\text{true}}}{k_{s,\text{true}}} = \left(\frac{\hat{h}_\text{es}}{h_\text{es}} \frac{h_\text{ek,n}}{\hat{h}_\text{ek,n}} \right)^3 \left(\frac{W_\text{end}'}{\hat{W}_\text{end}'} \bigg|_{x=1} \right)^2 \left(\frac{\hat{\psi}_n'(1)}{\psi_n'(1)} \right)^2 \frac{k_{nn}}{\hat{k}_{nn}} - 1, \tag{11}$$

where the hats (ˆ) once again denote the entities for the model of interest. The normalized deflection curve and its derivative for a uniform cantilever are known [12]. The derivative of the deflection curve for a cantilever with an arbitrary thickness profile is calculated using the analytical model for the static deflection of a non-uniform model, which was also used to derive eq. (4).

$$W_\text{end}'(x) = \frac{\int_0^x \frac{(x-1)}{h(x)^3} \mathrm{d}x}{\int_0^1 \int_0^x \frac{(x-1)}{h(x)^3} \mathrm{d}x \mathrm{d}x} \tag{12}$$
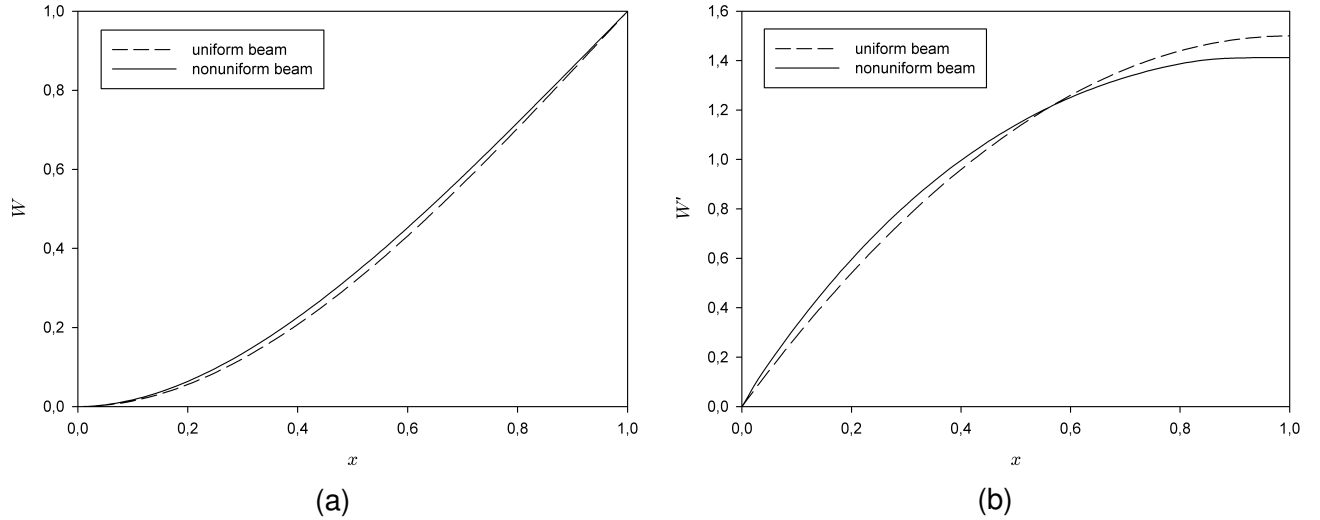

Figure 5: Deflection curves of uniform and non-uniform cantilevers under static loading in (a) and the derivative with respect to x, i.e. the slope of the cantilever, in (b).

The deflection curves and their derivatives with respect to x are given in Figure 5 for both the uniform and the measured thickness profiles. It can be observed that the slopes are considerably different near the free end, and this difference is squared in eqs. (10) and (11), so it may be important. The rotation of the mode shapes, $\psi_n'(1)$, i.e. the shape of the freely vibrating cantilever, also induces error in the Thermal Tune method. The slope at the free end of the cantilever is influenced by the profile of the beam, as was illustrated in Figure 3.

Table 5 presents the errors in the Thermal Tune estimated spring constant once again using the thickness profile from the SEM images as the "true" model. In contrast with the Sader method, the thermal method is significantly in error if a uniform probe model is used, even if the first mode is used in the calibration. The error becomes extremely unacceptable if the second or higher modes are used. In contrast, the linear and lumped models are acceptably accurate for the first mode but even they become very inaccurate if the third or higher modes are used.

δk_s	Mode 1	Mode 2	Mode 3	Mode 4
Uniform No Tip - Measured	15.31%	72.79%	160.93%	287.70%
Uniform + Tip - Measured	22.53%	71.88%	134.93%	214.03%
Linear and Lumped - Measured	6.32%	13.82%	35.79%	73.20%
Linear and Lumped #2 - Measured	4.64%	8.87%	28.21%	63.07%

Table 5: Error in the static stiffness estimated by the Thermal Tune method for various profiles as a function of the mode number used in the calibration. The model based on the measured profile was taken to be exact.

4 Conclusion

The thickness profile of a cantilever has a decisive influence on its static stiffness as well as its mode shapes. Two common atomic force microscope calibration methods were analyzed to see what influence this has on the calibration. The Sader method was found to accurately estimate the static stiffness of the probe under study, but only if the first mode was used in the calibration. We presume that similar trends would hold for other probes so long as the non-uniformity is not too drastic, so the Sader method seems to be quite a robust choice. On the other hand, the thermal method depends on the rotation of the cantilever under static and dynamic loading and so it was found to be very sensitive to the probe's non-uniformity. These results suggest that the thermal method should not be trusted unless the probe of interest is known to be uniform. A few simple models were explored in an effort to capture the effect of thickness nonuniformity. The models were found to reproduce the natural frequencies and mode shapes of the probe reasonably well, but calibration is sensitive to the model. The "linear and lumped" model did reduce the error in the Thermal Tune calibration somewhat, but even then the results showed that one may only be able to trust the calibration based on either the first or perhaps the second mode of the probe. Also, future works should seek to characterize other probes as was done here for the CSC38 probe, to see whether any of the models proposed here can account for the range of commonly encountered nonuniformities with sufficient fidelity.

5 Acknowledgments

6 Appendix

6.1 Parameterized profiles

$$h(x) = h_0 + h_1 x , \qquad 0 \leq x \leq 1 \tag{13}$$

$$\Delta m = \rho b L \int_0^1 h_\mathrm{measured}(x) - h(x)\mathrm{d}x \tag{14}$$

$$h(x) = \begin{cases} h_{\text{nom}} & 0 \le x < x_0 \\ h_{\text{nom}} + h_1\,(x - x_0) & x_0 \le x \le 1 \end{cases} \quad \text{with} \quad h_1 = \frac{h(1) - h_{\text{nom}}}{1 - x_0} \tag{15}$$

6.2 Ritz coefficients

$$M_{nn} = \rho b L (h_{\text{em}} m_{nn}) + \left[\frac{\pi}{4} \rho_f b^2 L \Gamma_{\text{r}}(\omega) \right] m_{nn} + m_{\text{tip}} \psi_n(1)^2 + \frac{I_{\text{tip}}}{L^2} \left(\psi_n'(1) \right)^2 \tag{16}$$

$$C_{nn} = \left[\frac{\pi}{4} \rho_f \omega b^2 L \Gamma_{\text{i}}(\omega) \right] m_{nn} \tag{17}$$

$$K_{nn} = \frac{Eb}{12L^3} (h_{\text{ek},n}^3 k_{nn}) \tag{18}$$

$$k_{nn} = \int_0^1 \left(\psi_n'' \right)^2 \mathrm{d}x, \qquad m_{nn} = \int_0^1 \left(\psi_n \right)^2 \mathrm{d}x \tag{19}$$

References

[1] G. Binnig, C. F. Quate, and C. Gerber. Atomic force microscope. *Physical Review Letters*, 56:930–933, 1986.

[2] L. Gross, F. Mohn, N. Moll, P. Liljeroth, and G. Meyer. The chemical structure of a molecule resolved by atomic force microscopy. *Science*, 325:1110–1114, 2009.

[3] Y. Sugimoto, P. Pou, O. Custance, P. Jelinek, M. Abe, R. Perez, and S. Morita. Complex patterning by vertical interchange atom manipulation using atomic force microscopy. *Science*, 322:413–417, 2008.

[4] A. Touhami, M. H. Jericho, and T. J. Beveridge. Atomic force microscopy of cell growth and division in staphylococcus aureus. *Journal of Bacteriology*, 186:3286–3295, 2004.

[5] Y. F. Dufrene. Towards nanomicrobiology using atomic force microscopy. *Nature Review Microbiology*, 6:674–680, 2008.

[6] S. Cross, Y. S. Jin, and J. Rao andf J. K. Gimzewski. Nanomechanical analysis of cells from cancer patients. *Nature Nanotechnology*, 2:780–783, 2007.

[7] J. E. Sader and L. White. Theoretical analysis of the static deflection of plates for atomic force microscope applications. *Journal of Applied Physics*, 74:1–5, 1993.

[8] J. E. Sader, I. Larson, P. Mulvaney, and L. White. Method for the calibration of atomic force microscope cantilevers. *Review of Scientific Instruments*, 66:3789–3798, 1995.

[9] M. S. Allen, H. Sumali, and P. C. Penegor. Experimental/analytical evaluation of the effect of tip mass on atomic force microscope calibration. *Journal of Dynamic Systems, Measurement, and Control*, Accepted, April 2009, DOI: 10.1115/1.4000160.

[10] J. L. Hutter and J. Bechhoefer. Calibration of atomic force microscope tips. *Review of Scientific Instruments*, 64:1868–1873, 1993.

[11] N. A. Burnham, X. Chen, C. S. Hodges, G. A. Matei, E. J. Thoreson, C. J Roberts, M. C. Davies, and S. J. B. Tendler. Comparison of calibration methods for atomic force microscopy cantilevers. *Nanotechnology*, 14:1–6, 2003.

[12] S. M. Cook, T. E. Schaeffer, K. M. Chynoweth, M. Wigton, R. W. Simmonds, and K. M. Lang. Practical implementation of dynamic methods for measuring atomic force microscpoe cantilever spring constants. *Nanotechnology*, 17:2135–2145, 2006.

[13] J. H. Ginsberg. *Mechanical and Structural Vibrations: Theory and Applications*. John Wiley & Sons, 2001.

[14] J. E. Sader, J. W. M. Chon, and P. Mulvaney. Calibration of rectangular atomic force microscope cantilevers. *Review of Scientific Instruments*, 70:3967–3969, 1999.

[15] M. K. Ghatkesara, E. Rakhmatullinab, H. P. Langa, C. Gerbera, M. Hegnera, and T. Brauna. Multiparameter microcantilever sensor for comprehensive characterization of newtonian fluids. *Sensors and Actuators B: Chemical*, 135:133–138, 2008.

[16] J. E. Sader. Frequency response of cantilever beams immersed in viscous fluids with applications to the atomic force microscope. *Journal of Applied Physics*, 84:64–76, 1998.

[17] M. S. Allen, H. Sumali, and P.C. Penegor. Effect of tip mass on atomic force microscope calibration by thermal method. In *27th International Modal Analysis Conference, Orlando, Florida*, 2009.